

Antonio Sciarretta

Angular Momentum and Spin in a Local-Realistic Model of Quantum Mechanics

the date of receipt and acceptance should be inserted later

Abstract This paper presents an extension of the realistic, stochastic, and local model for Quantum Mechanics published in [1]. The proposed model reproduces nonrelativistic quantum mechanics (QM) results without using its mathematical formulation, but using only integer-valued quantities and operations on probabilities, in particular assuming a discrete spacetime under the form of a lattice. Individual particle trajectories are described as random walks. Transition probabilities are simple functions of a few quantities that are either randomly associated to the particles during their preparation, or stored in the lattice nodes they visit during the walk. QM predictions are retrieved as probability distributions of similarly-prepared ensembles of particles. This paper adds the description of spin and spin entanglement, including the description of Stern-Gerlach apparatuses and Bell test experiments.

1 Introduction

In [1,2], we have proposed a model mimicking quantum mechanics (QM) with local, realistic, and stochastic features.

In the proposed model, the results of nonrelativistic spinless QM systems have been interpreted as probability distributions of similarly-prepared ensembles of particles that are emitted by one or multiple sources. At a given time, individual particles have definite values for position and momentum, among other observables, thus fulfilling *realism*.

The *stochastic* behavior that is manifested by the empirical evidence of QM is explained by assuming a fundamental randomness both in preparation and in particles trajectories. The emergence of QM behavior is a consequence

A. Sciarretta
34, rue du Chateau, 92500 Rueil Malmaison, France
Tel.: +33 951201691

of the particular rules of motion chosen. The motion of individual particles and their interaction with external forces take place on a discrete spacetime under the form of a lattice. Particle trajectories are asymmetric random walks, with transition probabilities being simple functions of a few quantities that are either randomly attributed to the particles during their preparation, or stored in the lattice nodes that the particle visits during the walk.

The lattice-stored information is progressively built as the nodes are visited by successive emissions. This process, where particles leave a “footprint” in the lattice that is used by subsequent particles, is ultimately responsible for the QM behavior. Therefore the interactions between subsequent emissions fulfill *localism*, albeit through the mediation of the lattice. Interference and the Born rule emerge as a consequence of this mechanism.

In contrast with the orthodox view that QM is complete and that only probability distributions can be described, not the individual events that perhaps contribute to the observed statistical averages, “realistic” interpretations have been sought since the early quantum history [3,4,5,6]. Possibly the best-known realistic theory is the De Broglie–Bohm mechanics [7,8], which describes individual particle trajectories that are deterministic for a given initial position. In contrast to our proposed model, the Bohmian mechanics explicitly appeals to a nonlocal mechanism, with the guiding wave or the quantum potential instantaneously influencing the particle trajectory far away. Also in the emergence of the stochastic behavior leading to the collective patterns observed, the proposed model contrasts with Bohmian mechanics since, in the latter, probability represents only the uncertainty of the initial state of the particle rather than also randomness in the trajectories.

Another class of realistic and stochastic models attempt at simulating QM with random walks, an idea that has its origin in the path integral formalism and the chessboard model introduced by R. Feynman [9]. Since then, many works have appeared in the literature to retrieve the Schrödinger equation from a random walk process, including those of G. Ord [10,11,12] and subsequent refinements [13], as well as different yet related approaches [14]. While these approaches are able to reproduce the emergence of a Schrödinger-type equation, the Born probability rule is not explained in such models.

Following E. Nelsons seminal work [15], another approach has consisted of showing the emergence of the Schrödinger equation from a stochastic equation of motion [16,17,18,19,20]. Such derivation, however, is founded on the assumption of reversible diffusion or competing diffusion-antidiffusion processes, leading to a key osmotic velocity that depends on the probability field it concurs in building. As such, these theories are not coping with localism.

An event-based class of models have been recently proposed [21,22,23] that embody quantum behavior into the constitutive models of the detectors and other devices, mostly using deterministic learning machines that generate events according to QM. This approach captures all of the features of realism, localism, and randomness. However, QM behavior is not obtained as an intrinsic characteristic of the particles trajectories but as a result of their interaction with the experimental apparatus, while in our proposed approach

detectors and other devices are assumed to be simple counters and do not participate in building the interference patterns.

Other suggestions to make QM behavior emerge from discrete time evolution [24] or vacuum fluctuations [3] were not pursued to the end, to our best knowledge. It is further noteworthy to mention that in the proposed model the lattice is only the support for particle motion, not for wave functions or other mathematical operators [25, 26]. In a certain sense, the lattice plays the role of the guiding wave assumed by de Broglie–Bohm theory and evidenced by some macroscopic experiments [27]. However, the QM behavior is not produced by a single particle interacting with the wave interface (walker in [27]), but it is generated by successive emissions of the same ensemble. It is further noteworthy to mention that QM behavior is not reproduced by appealing to probabilistic cancellation, nor to other definitions of negative probabilities.

Despite its compactness, the proposed model has proven sufficient to reproduce various QM scenarios, from free particle preparations to various external forces (free faller, harmonic oscillator), infinite potential walls (particle in a box), finite potential walls (Delta potential) with quantum tunneling. In addition, it has been shown that Bell’s inequalities are violated in a Bell test with momentum-entangled pairs of particles and QM results are reproduced, despite the fact that local theories are generally thought to be ruled out by Bell’s theorem. In fact, the proposed model is not of the form postulated by Bell’s assumptions, thus it is not forbidden by Bell’s theorem to violate Bell’s inequalities.

In this paper, we aim at extending the model to cover spin ($1/2$, at least). The main characteristic that distinguishes quantum spin from classical magnetic moment behavior is probably the quantization of the former after a measurement, e.g., by a Stern-Gerlach (SG) apparatus, is performed. This behavior is described in standard QM using matrices and eigenvectors. In alternative theories, spin has been derived from path integrals [28] and Nelson’s stochastic mechanics [29, 30]. The local-realistic mechanism proposed here only involves a few additional quantities carried on by the particles. These variables are subject to stochastic preparation at sources and time evolution, including interaction with the lattice nodes storing the information about the magnetic field.

The proposed model is also used to demonstrate spin entanglement in addition to momentum entanglement already incorporated in [1]. Perhaps the only previous attempt to reproduce Malus’ law and QM predictions in a local-realistic context is that of the aforementioned event-based models [23]. There, the key notion is that of time delay between particle arrivals at the detectors of a Bell-type experiment, so that coincidences are counted only if two particles arrive at roughly the same time. Such a time delay is heuristically designed and explained with the properties of the apparatus. Instead, in the proposed model, the time-of-fly is a natural consequence of the rules of motion in the presence of magnetic forces and is a stochastic quantity due to stochastic preparations.

The paper is organized as follows. In Sect. 2 a summary of the three-dimensional spinless model is presented, with some additional considerations with respect to [1]. In particular, quantization of angular momentum is dis-

cussed in Sect. 3. Then in Sect. 4 the additional rules for spin are introduced, both for homogeneous and inhomogeneous (SG) fields. Two-particle spin entanglement is discussed in Sect. 5.

2 Summary of the Local-Realistic Model for a Spinless Particle

In this section, we summarize the rules for particle emissions (Sect. 2.1), microscopic motion (Sect. 2.2), and how probability densities are derived from them (Sect. 2.3). The reader is referred to [1] or its companion paper [2] for more detail.

2.1 Lattice and particle emissions

The lattice is composed of three spatial dimensions $x = \{x_d\} \in \mathbb{Z}^3$, and one temporal dimension $n \in \mathbb{N}$. Each of the spatial dimensions is characterized by the same fundamental length and acts independently.

Source preparation fixes the source position $x_0 = \{x_{0d}\} \in \mathbb{Z}^3$, the source phase $\epsilon = \{\epsilon_d\} \in \mathbb{Q}^3$, the source momentum $v_0 = \{v_{0d}\} \in \mathbb{Q}^3$, and the source (momentum) polarization $\rho = \{\rho_d\} \in \mathbb{Q}^3$. The latter two quantities are further subject to the conditions $\sum_{d=1}^3 \rho_d^2 = 1$, $\sum_{d=1}^3 v_{0d}^2 \leq 1$.

Source setting consists in defining the number of sources N_s , their location $x_0^{(k)}$, probabilities $P_0^{(k)}$ (such that $\sum_k P_0^{(k)} = 1$), and phase $\epsilon^{(k)}$. In the special yet common case of independent directions, we shall simplify the notation (with some abuse), and write $P_0(x) = \prod_{d=1}^3 P_{0d}(x_d)$ and $\epsilon(x) = \sum_{d=1}^3 \epsilon_d(x_d)$.

2.2 Microscopic motion

Microscopic motion is defined by a set of rules involving quantities carried by particles and quantities carried by lattice node (subscript xt).

The particle-carried quantities (or “counters”) are: its span $\ell = \{\ell_d\} \in \mathbb{Z}^2$, lifetime $t \in \mathbb{N}$, momentum $v = \{v_d\} \in \{-1, 0, 1\}^3$, momentum propensity $\mathbf{v} := \mathbb{E}[v]$, “energy” $e := \mathbb{E}[v^2]$, quantum momentum $v_Q = \{v_{Qd}\} \in \mathbb{Q}^3$, momentum due to external forces $v_F = \{v_{Fd}\} \in \mathbb{Q}^3$.

Particles exchange momentum-mediating entities called “bosons” with the lattice, according to the mechanism illustrated below. External-force bosons (FB) carry a momentum $f = \{f_d\} \in \mathbb{Q}^3$, while quantum particle bosons (PB) carry momenta $w^{(\cdot)} \in \mathbb{Q}$ and their own lifetime $n - n_{QR}^{(\cdot)}$, where $n_{QR}^{(\cdot)}$ is the iteration of last quantum reset (see below).

The particle's motion rules are summarized as

$$t[n] = t[n-1] + 1, \quad t[n_0] = 0 \quad (1)$$

$$\ell_d[n] = \ell_d[n-1] + v_d[n], \quad \ell_d[n_0] = 0 \quad (2)$$

$$x_d[n] = x_{0d} + \ell[n] \quad (3)$$

$$\mathbb{P}(v_d = \pm 1) = \frac{e_d \pm \mathbf{v}_d}{2}, \quad \mathbb{P}(v_d = 0) = 1 - e_d \quad (4)$$

$$e_d[n] = \frac{1 + \mathbf{v}_d^2[n]}{2} \quad (5)$$

$$\mathbf{v}_d[n] = v_{Qd}[n] + v_{Fd}[n] \quad (6)$$

$$v_{Fd}[n] = \sum_{n'=n_0+1}^n f_d(x[n'], n') \quad (7)$$

$$v_{Qd}[n] = v_{0d} - \rho_d^2 \sum_{\ell} \sum_{\lambda \neq \ell} w^{(\ell\lambda)}[n] \quad (8)$$

$$w^{(\ell\lambda)}[n] = w^{(\ell\lambda)}[n-1] \cdot \left(1 - \frac{1}{2 \left(n - n_{QR}^{(\ell\lambda)} \right)} \right) \quad (9)$$

Equations (1)–(3) describe the increment of lifetime, span, and position as a function of momentum. Equations (4)–(5) relate the probability distribution of momentum to momentum propensity. Equation (6) states that momentum propensity is the sum of two contributions, due to quantum, resp. external forces. External forces are described by interactions with the lattice, where each node can be occupied by a force boson. When a particle visits the node, it captures the resident FB and incorporates its momentum as described in (7). A new boson is then recreated at the node. In (8), quantum momentum is initially set to the source momentum and then build up from an exchange of bosons and their momenta between the particle and the lattice. The dynamics of the PB-momentum is given in (9).

Lattice-carried quantities are the span trace $\lambda_{xt} = \{\lambda_{d,xt}\} \in \mathbb{Z}^3$ and the phase trace, $\epsilon_{xt} \in \mathbb{Q}^3$, which represent the memory of the span and phase carried by the last particle that has visited the node x with lifetime t . Additionally, the exchange with particles generate quantum lattice bosons (LB), carrying momenta $\omega_{xt}^{(\cdot)} \in \mathbb{Q}$, whose dynamics read

$$\omega_{xt}^{(\ell\lambda)}[n] = \omega_{xt}^{(\ell\lambda)}[n-1] \cdot \left(1 - \left(\frac{\omega_{xt}^{(\ell\lambda)}[n_{QR}^{(\ell\lambda)}]}{n - n_{QR}^{(\ell\lambda)}} \right)^2 \right). \quad (10)$$

Rules (1)–(10) are partially overcome in case of a quantum reset or an external reset. A Quantum Reset (QR) occurs (at iteration $n_{QR}^{(\ell\lambda)}$) when $\ell_d \neq \lambda_{d,xt}$ for at least one dimension d . If it is the case, the following exchanges

apply:

$$w^{(\ell\lambda)} \xleftarrow{QR} \frac{\omega_{xt}^{(\ell\lambda)}}{\sum_{d=1}^3 \rho_d^2 \delta_d^{(\ell\lambda)}} \quad (11)$$

$$\omega_{xt}^{(\ell\lambda)} \xleftarrow{QR} \sum_{d=1}^3 \delta_d^{(\ell\lambda)} v_{Qd} - \epsilon^{(\ell\lambda)} \quad (12)$$

$$\ell_d \xleftrightarrow{QR} \lambda_{d,xt} \quad (13)$$

$$\epsilon \xleftrightarrow{QR} \epsilon_{xt} \quad (14)$$

where $\delta_d^{(\ell\lambda)} := |\ell_d - \lambda_{d,xt}|$ is the path difference, $\epsilon^{(\ell\lambda)} := \epsilon - \epsilon_{xt}$ is the phase difference.

Rules (11)–(12) state that the QR creates a new momentum-carrying LB, labeled $\ell\lambda$ to unambiguously identify the information carried by the particle, resp., the lattice node. The new LB replaces the old one of the same type, which is transferred to the particle and becomes a particle boson (PB). Rules (13)–(14) describe the exchange of counters between the particle and the lattice.

An External Reset (ER) occurs when an external-force boson is captured, and is defined by the rules

$$v_{d0} \xleftarrow{ER} v_d \quad (15)$$

$$\ell_d \xleftarrow{ER} \ell_d - 2f_d \frac{\sum_{d'=1}^3 \ell_{d'} f_{d'}}{\sum_{d'=1}^3 f_{d'}^2} \quad (16)$$

$$\epsilon \xleftarrow{ER} \epsilon + 1. \quad (17)$$

Although not necessary, rule (15) is introduced here for the sake of model elegance. It states that each ER can be seen as a new emission, thus removing the special role of sources that are now seen as just the nodes where the last interaction has taken place. Rule (16) generalizes the 1D situation where the span's sign is inverted at each external interaction. Rule (17) adds a π phase angle after each interaction.

2.3 Probability densities

The source position, momentum, and polarization are treated as random variables. In particular, the probability density function of the source momentum is $\rho(v_{d0}) = (1/2), \forall d$.

Stochastic preparation implies that \mathbf{v} and thus x are random variables, too. We aim at evaluating the probability mass function of the position for an ensemble of similarly-prepared particles. Unfortunately, it is generally not possible to explicitly evaluate $\rho(x;t)$. However, as discussed in [1], for sufficiently large times we can use the approximation $\rho(x;t) \approx \rho(\mathbf{x};t)$, where $\mathbf{x} \in \mathbb{R}$ is the expected value of the position.

We describe in the rest of this section the procedure to evaluate the joint pdf's $\rho(\mathbf{x}; t)$ and $\rho(\mathbf{v}_Q)$ in the presence of quadratic potentials and/or potential barriers, geometrical constraints.

2.3.1 Quadratic potentials

It was shown in [1] that, in case of a quadratic potential, the expected motion is given by

$$\mathbf{x}_d = A_d(t)x_{0d} + B_d(t)\mathbf{v}_{Qd} + C_d(t) \quad (18)$$

and

$$\mathbf{v}_{Qd} = v_{0d} - \rho_d \sum_i \sum_{j \neq i} \sqrt{P_0^{(i)} P_0^{(j)}} \frac{\sin(\arg)}{\pi \sum_{d=1}^3 \rho_d \delta_d^{(ij)}} \quad (19)$$

$$(\arg) = \pi \sum_{d=1}^3 \delta_d^{(ij)} \frac{\mathbf{x}_d - A_d(t) \frac{x_{0d}^{(i)} + x_{0d}^{(j)}}{2} - C_d(t)}{B_d(t)} - \pi \epsilon^{(ij)}. \quad (20)$$

where $A(t)$, $B(t)$, and $C(t)$ are functions of lifetime whose form depends on the EB momentum (external force) $f(x, t)$. For a free particle, $A = 1$, $B = t$, $C = 0$; a free faller, $A = 1$, $B = t$, $C = ft^2/2$; an harmonic oscillator, $A = \cos \Omega t$, $B = \sin \Omega t / \Omega$, $C = 0$.

The joint pdf of the positions is found by applying the rule

$$\rho(\mathbf{x}; t) = \frac{1}{2} \left| \frac{\partial(v_{01}, \dots, v_{03})}{\partial(\mathbf{x}_1, \dots, \mathbf{x}_3)} \right|, \quad (21)$$

yielding

$$\rho(\mathbf{x}; t) = \frac{1 + \sum_i \sum_{j \neq i} \sqrt{P_0^{(i)} P_0^{(j)}} \cos(\arg)}{\prod_{d=1}^3 2|B_d(t)|} \quad (22)$$

In [1] it was shown as well that the Schrödinger equation and Born rule can be retrieved from (22).

Similarly, the joint pdf of the momenta is evaluated as

$$\rho(\mathbf{v}_Q; t) = \frac{1}{2^3} \left(1 + \sum_i \sum_{j \neq i} \sqrt{P_0^{(i)} P_0^{(j)}} \cos \left(\pi \sum_{d=1}^3 \delta_d^{(ij)} \mathbf{v}_{Qd} - \pi \epsilon^{(ij)} \right) \right) \quad (23)$$

2.3.2 Potential barriers

“Potential barriers” are particular nodes at which the FB-momentum is a function of the particle's momentum propensity. Geometrically, each of such nodes is characterized by the parameter $a := \{a_d\} \in \mathbb{Q}^3$, such that $\sum_{d=1}^3 a_d^2 = 1$. Each time a particle hits the barrier, it gains an FB-momentum

$$f_d[n] = -2 \left(\sum_{d'=1}^3 a_{d'} \mathbf{v}_{d'}[n] \right) a_d \quad (24)$$

For example, for a 1D potential barrier, $f = -2\mathbf{v}$.

Inserting (24) in (16) reveals that at potential barriers the ER condition activates a span update $\ell_d \xleftarrow{ER} \ell_d - 2a_d \left(\sum_{d'=1}^3 a_{d'} \ell_{d'} \right)$. Consequently, each barrier location can be described as generating a “virtual mirror” of each actual source. If x_B are the barrier locations, then the virtual mirror of x_0 is $x_v(x_0) = x_0 + 2a \left(\sum_{d'=1}^3 a_{d'} (x_{Bd} - x_{0d}) \right)$. For example, for a 1D potential barrier, $x_v = 2x_B - x_0$. In case of multiple barrier locations, multiple virtual sources are generated. This is the case of the “particle-in-a-box” scenario, which has been treated in [1].

2.3.3 Geometrical constraints

A “geometrical constraint” is active when the particle is forced to follow a particular combination of lattice nodes (a line or a surface). There are several ways to describe such situations in the proposed model. One possibility, mentioned in [2], is to attribute $f = 0$ on the line/surface, while everywhere else the force (24) applies. Another method, simpler to be treated, is to assume particular (momentum-propensity-dependent) forms of $A(t)$, $B(t)$, and $C(t)$, such that the geometrical constraint is enforced. If for example, direction d is to be ignored to represent a 2D scenario, we will just take $B_d = C_d = 0$ in (18).

2.4 Special preparations

Using the result of Sect. 2.3.3, we refer in this section to a 1D scenario omitting the subscript d , and we derive some results for a few special preparations, to be used later.

2.4.1 “Wavepacket” preparations

Wavepackets can be prepared by setting a finite number N_s of sources at adjacent nodes centered at $x = 0$. The source phase is set as $\epsilon_d(x) = mx$, with $m \in [0, 1]$. The probability is set as constant, $P_0(x) = 1/N_s$ for a “plane wave” preparation or as $P_0(x) = \frac{1}{2^{N_s-1}} \binom{N_s-1}{x + \frac{N_s-1}{2}}$ for a “Gaussian wave” preparation with variance $(N_s - 1)/4$.

When (23) is applied, one obtains a probability density that peaks for $\hat{v}_Q = m$. The peak intensity increases with N_s for plane waves, with $\sqrt{N_s}$ for Gaussian waves, as it is the case with QM states.

2.4.2 Periodic sources

Diffraction gratings are prepared with a large number N_s of equally-probable sources that are periodically arranged with period a , with source phase still set as $\epsilon_d(x) = mx$, where $m = 0$ holds for phased sources and $m = 1$ for alternating sources.

When (23) is applied, one obtains that

$$\lim_{N_s \rightarrow \infty} 1 + \sum_{i=1}^{N_s} \sum_{j=i+1}^{N_s} \frac{1}{N_s} \cos(\pi|i-j|(av_Q - m)) = III_{2/a}(v_Q - m/a), \quad (25)$$

where $III_T(\cdot)$ is the Dirac comb of period T . Since this function peaks at nT , $n = -\infty, \dots, \infty$, (23) has peaks at $\hat{v}_Q^{(n)} = (2n + m)/a$. Of course, only values $\in [-1, 1]$ are admissible. For $a = 1$ one retrieves the result of the previous section since only the order $n = 0$ is admissible in this case.

2.4.3 Stationary states

Stationary states are those particular source preparations whose evolution preserves the source probability distribution. An implicit expression for such probability function P_{ss} is

$$P_{ss}(x) = \frac{1 + \sum_i \sum_{j \neq i} \sqrt{P_{ss}(i)P_{ss}(j)} \cos(arg)}{2|B(t)|}, \quad (26)$$

$$(arg) = \pi|i-j| \frac{x - A(t)\frac{i+j}{2} - C(t)}{B(t)} - \pi\epsilon(x). \quad (27)$$

3 Angular momentum

The description of angular momentum phenomena does not require in principle anything but the rules defined in the previous section for three-dimensional scenarios. However, the treatment can be substantially simplified if the dimensions are reduced to two or even one, assuming particular geometric constraints. The treatment of such constraints needs some preliminary considerations at this stage.

3.1 2D Free particle

In this scenario the particle is free in two dimensions x_1, x_2 , while $x_3 = 0$. The expected motion is $\mathbf{x}_d = x_{0d} + \mathbf{v}_{Qd}t$, $d = 1, 2$.

Ensemble results for an angular momentum eigenstate preparation are compared with those of quantum mechanics (theoretical values) obtained by using the propagator

$$K^{(FP2)}(x_1, x_2, t | x_{01}, x_{02}) = \frac{1}{2it} \exp\left(\frac{i\pi(x_1 - x_{01})^2}{2t}\right) \exp\left(\frac{i\pi(x_2 - x_{02})^2}{2t}\right). \quad (28)$$

In particular, we are interested in probability distributions of the expected values of angular momentum and energy, $\rho(\mathbf{J}_3; t)$ and $\rho(\mathbf{E}; t)$, where $\mathbf{J}_3 \triangleq \mathbf{x}_1 \mathbf{v}_{Q2} - \mathbf{x}_2 \mathbf{v}_{Q1}$ and $\mathbf{E} \triangleq (\mathbf{v}_{Q1}^2 + \mathbf{v}_{Q2}^2)/2$.

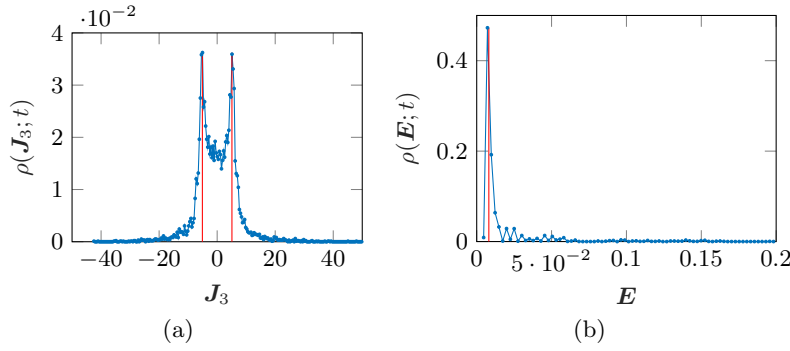


Fig. 1 Angular momentum (left) and energy (right) distributions (blue points) and theoretical values (red) for $N_p = 1000$, $t = 60$ (free particle, angular momentum eigenstate, $l = 16$, $k = 0.4$).

3.1.1 Angular momentum eigenstate

In such scenario the source probability and phase are prepared so to represent the QM initial state $\psi_0^{(l)} = e^{i\phi} J_l(kr)$, where J_l is the Bessel function of the first kind with order l , k is the energy eigenvalue, $\phi \triangleq \arctan(x_2/x_1)$ and $r \triangleq \sqrt{x_1^2 + x_2^2}$. In particular, $P_0(x) = J_l(kr)^2$ and $\epsilon(x) = l\phi$.

The theoretically expected pdf is obtained by applying the propagator (28) to ψ_0 . Since this is a stationary state, the theoretically expected pdf is obtained as $\rho(\mathbf{x}) = |\psi_0(\mathbf{x})|^2$ and is a function of r alone, not of ϕ .

Figure 1 shows the distribution $\rho(\mathbf{J}_3; t)$ after $t = 60$ iterations with $l = 16$ and $k = 0.4$. It shows two peaks at values $\pm l/\pi$, which correspond to the eigenvalues of ψ_0 in lattice units. On the other hand, the distribution $\rho(\mathbf{E}; t)$ peaks at the value $(k/\pi)^2/2$. These result clearly match the predictions of QM.

3.2 Particle on a ring (1d periodic motion)

In this scenario the particle is confined on a set of lattice nodes such that $\text{round}[\sum_{d=1}^2 x_d^2] = r^2$ and $x_3 = 0$, where r is the ring radius (an integer). Consequently, the only relevant motion is that along the ring, $r\phi$, where ϕ is the standard polar angle measured clockwise from the $(0, r)$ point. This situation is equivalent to a 1D free periodic motion described by the polar coordinate ϕ . The expected motion is $\phi(t) = \arcsin(\sin(\mathbf{v}_{Q\phi} t/r))$. The expected value of the angular momentum is $\mathbf{J}_3 = r\mathbf{v}_{Q\phi}$, and that of energy is $\mathbf{E} = \mathbf{v}_{Q\phi}^2/2$.

Ensemble results for single-source, plane-wave, and stationary-state preparations are compared with those of quantum mechanics (theoretical values) obtained by using the propagator

$$K^{(PR)}(\phi, t|\phi_0) = \sum_{m=-\infty}^{m=\infty} \left(\frac{\pi r^2}{2\pi i t} \right)^{1/2} \exp\left(\frac{i\pi r^2 (\phi - \phi_0 - 2\pi m)^2}{2t} \right). \quad (29)$$

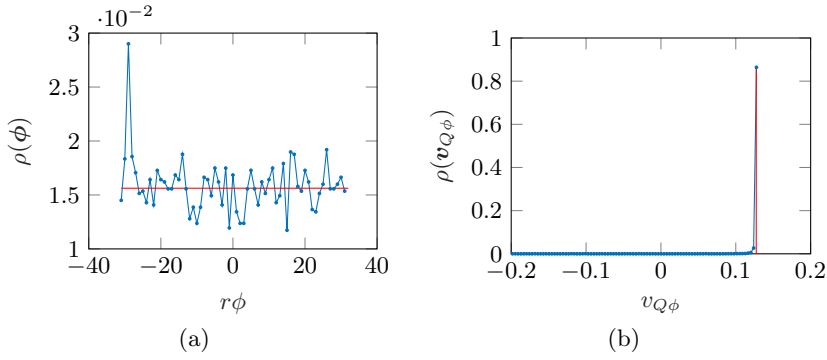


Fig. 2 Position (left) and momentum (right) distributions and theoretical values (red) for $N_p = 5000$, $t = 1000$ (particle on a ring, plane wave preparation, $r = 10$, $m = 4$).

This propagator is equivalent to that of a 1D free motion with an infinity of equally-probable virtual sources separated by $2\pi r$. Indeed, in the proposed model quantum forces arise, even in the presence of a single physical source, because a given node on the ring can be visited by particles having looped through the ring a different number of times, thus with a peripheral span ℓ_ϕ that may differ for a multiple of the ring circumference.

3.2.1 Single source

The source setting is $r\phi_0 = 0$, $P_0 = 1$, and $\epsilon = 0$. The theoretically expected pdf is found by applying the propagator (29) to the initial state $\psi_0 = \delta(\phi_0)$.

Note that this case is equivalent to that of a free 1D particle with an infinity of periodic sources with $a = 2\pi r$, $m = 0$ [1]. Based on (25), the pdf of the momentum has Dirac peaks at $\hat{v}_{Q\phi}^{(n)} = n/\pi r$, with $n = 0, \pm 1, \pm 2, \dots$. Consequently, the kinetic energy has peak values $\hat{E}^{(n)} = n^2/(2\pi^2 r^2)$, and the angular momentum has peak values $\hat{J}_3^{(n)} = n/\pi$, in agreement with QM predictions in lattice units. Simulation results are obvious and not shown.

3.2.2 Plane wave

A plane-wave preparation is obtained to represent the QM initial state $\psi_0 = 1/\sqrt{2\pi r} e^{im\phi}$. In particular, $P_0(\phi) = 1/([2\pi r] + 1)$ and $\epsilon(\phi) = m\phi$.

The theoretically expected pdf is found by applying the propagator (29) to the initial state and is equal to $\rho(\phi; t) \approx 1/([2\pi r] + 1)$.

Figure 2-a shows the frequency of arrival after $t = 1000$ iterations with $r = 10$ and $m = 4$. Figure 2-b shows the distribution of the quantum momentum. The frequency clearly tends to the theoretical pdf, while the momentum clearly tends to the theoretically allowed value $m/(\pi r)$.

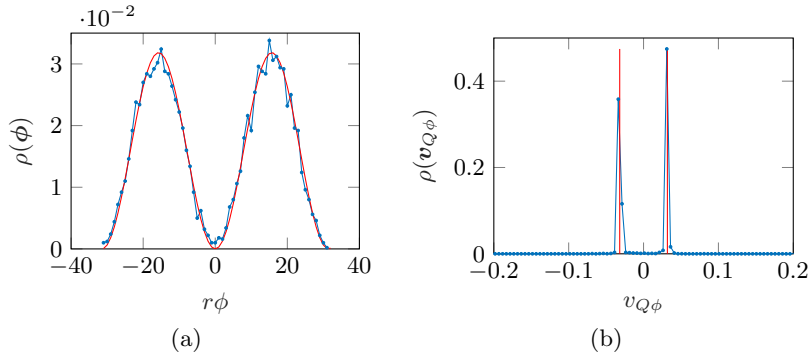


Fig. 3 Position (left) and momentum (right) distributions and theoretical values (red) for $N_p = 5000$, $t = 1000$ (particle on a ring, stationary state preparation, $r = 10$, $n = 1$).

3.2.3 Stationary state

In this scenario the source probability and phase are prepared so to represent QM initial states $\psi_0^{(n)} = 1/\sqrt{\pi r} \sin(n\phi_0)$ for $n \in \mathbb{Z}$ odd and $\psi_0^{(n)} = 1/\sqrt{\pi r} \cos(n\phi_0)$ for $n \in \mathbb{Z}$ even.

Since these are stationary states, the theoretically expected pdf is obtained as $\rho(\phi; t) = |\psi_0(\phi)|^2$. This function has peaks at $\hat{\phi}^{(m)} = \pm(1+2m)/2n$, $m = 0, \dots, n-1$ for n odd and $\hat{\phi}^{(m)} = \pm m/n$, $m = 0, \dots, n$ for n even. The theoretical momentum pdf is a Dirac delta function $\rho(v_{Q\phi}) = \delta(v_{Q\phi} \pm n/\pi r)$ with two symmetric eigenvalues.

Figure 3-a shows the frequency of arrival after $t = 1000$ iterations with $r = 10$, $n = 1$. Figure 3-b shows the distribution of the peripheral momentum. The frequency clearly tends to the theoretical pdf, while the momentum tends to the theoretically allowed values $\pm n/(\pi r)$.

4 Spin $\frac{1}{2}$

A spin mechanism is now superimposed to the microscopic motion mechanism treated in the previous sections. The momentum quantities v_0 , \mathbf{v} , and v have their spin counterparts s_0 , \mathbf{s} , and s . The (momentum) polarization ρ has its spin counterpart in the (spin) polarization μ . The latter two quantities might actually coincide: at the present stage of the model development, we do not have reasons to distinguish them but for their naming.

4.1 Microscopic motion

Particles are emitted with additional properties denoted as “source spin”, $s_0 \in \mathbb{Q}$ and source polarization, $\mu_0 := \{\mu_{d0}\} \in \mathbb{Q}^3$, such that $\sum_{d=1}^3 \mu_{d0}^2 = 1$.

During particles evolution, spin is prone to change at each time the particle experience a magnetic field, which is represented under the form

$B := \{\lambda_d\}B_M$, such that $\sum_{d=1}^3 \lambda_d^2 = 1$. Clearly, λ represents the unit vector along which the physical field is directed. The quantity B_M represents the magnitude of the magnetic field in lattice units.

The quantity denoted as spin, $s \in \mathbb{Q}$, varies during the particles evolution according to the rules

$$s[n] = \text{sign}(s_0 + \mathbf{s}[n]) \quad (30)$$

$$\mathbf{s}[n] = \sum_{d=1}^3 \mu_d[n] \lambda_d[n], \quad (31)$$

where $\mu := \{\mu_d\} \in \mathbb{Q}^3$ is the particle's polarization. We define for later use $s_\mu := \sum_{d=1}^3 \mu_{d0} \lambda_d^1$.

The evolution of the polarization follows the rule²

$$\begin{aligned} \mu_d[n+1] = & \mu_d[n] - \gamma \mu_M B_M (\mu_{d+1}[n] \lambda_{d+2}[n] - \mu_{d+2}[n] \lambda_{d+1}[n]) + \\ & - B_D s[n] \{ -(1 - \mu_d^2[n]) \lambda_d[n] + \mu_d[n] (\mu_{d+1}[n] \lambda_{d+1}[n] + \mu_{d+2}[n] \lambda_{d+2}[n]) \}, \end{aligned} \quad (32)$$

with $\mu_d[n_0] = \mu_{d0}$. The quantity μ_M represents the magnitude of the magnetic moment of the particle, and the dimension indexes must be taken as modulo three. The quantity γ represents the gyromagnetic ratio, while B_D represents a damping coefficient, which is assumed to be induced by external magnetic forces (see below). Note that, if the λ_d 's are constant, the sum \mathbf{s} evolves with iterations by virtue of (32) as

$$\mathbf{s}[n+1] = \mathbf{s}[n] - B_D s[n] (\mathbf{s}^2[n] - 1). \quad (33)$$

When an external boson is captured, besides the actualization of its momenta and spans (15)–(17), the particle undergoes an External Reset (ER) of its polarization,

$$\mu_d \xleftarrow[\text{ER}]{} s |\mu_d|. \quad (34)$$

Assuming that λ is constant, the magnetic force (external boson momentum) due to spin is described in analogy to the classical expression,

$$f_d[n] = -\mu_M \sum_{d'=1}^3 \mu_{d'}[n] \frac{\partial B_M}{\partial x_d}[n] \lambda_{d'}[n]. \quad (35)$$

We shall assume for later use that B_M is parameterizable as $\partial B_M / \partial x_d := B_F \nu_d$, with $\sum_{d=1}^3 \nu_d^2 = 1$. The force is thus directed along the $\nu := \{\nu_d\}$ direction and we can define its magnitude as $f_\nu[n] = -\mu_M B_F \mathbf{s}[n]$. As anticipated above, we further assume that the damping coefficient B_D is somehow related to B_F , so that, when no magnetic forces are experienced, $B_D = 0$.

¹ This quantity clearly corresponds to the cosine of the angle between the two directions μ_0 and λ .

² Note that this rule mimics the Landau–Lifshitz equation.

4.2 Probability densities

We aim at evaluating the pmf $\rho(s)$, which results from the particular preparation at the source and the nature of the magnetic field experienced by the ensemble of particles. We shall consider first a preparation (“pure state”) for which the source spin $s_0 = U[-1, 1]$, while the source polarization has a definite value μ_0 .

4.2.1 Homogeneous field

If the magnetic field $B_d = B_M \lambda_d$ is homogeneous in space (though possibly variable with time), no magnetic force is experienced, thus $B_F = B_D = 0$. If the field is also constant, (33) states that \mathbf{s} does not change with the iterations and thus is always equal to its initial value $s_\mu = \sum_{d=1}^3 \mu_{0d} \lambda_d$.

From (30), we have that s is also constant and

$$s[n] = \begin{cases} 1, & s_0 > -s_\mu \\ -1, & s_0 < -s_\mu \end{cases}. \quad (36)$$

The probability of spins up is thus evaluated as

$$\rho(1) = \Pr(s = 1) = \frac{1 + s_\mu}{2} = \frac{1 + \cos(\mu_0, \lambda)}{2}, \quad (37)$$

and is easily generalized to the case of a variable field, in perfect agreement with QM prediction.

The meaning of the polarizations in the model can be now clarified. If the field is along one particular direction d , then $\lambda_d = 1$, and consequently $\rho(1) = (1 + \mu_d)/2$, $\rho(-1) = (1 - \mu_d)/2$. The expectation value of the spin is therefore $\mathbf{s} = (1)(1 + \mu_d)/2 + (-1)(1 - \mu_d)/2 = \mu_d$. Thus the d -polarization represents the standard QM quantity $\langle S_d \rangle$, that is, the expected value of the spin measured along the d direction.

It should be also apparent that the standard QM spinor formulation of a spin state is represented in the model by the vector quantity

$$\chi = \left(\sqrt{\frac{1 + \mu_3}{2}}, \frac{\mu_1 - i\mu_2}{\sqrt{2}\sqrt{(1 + \mu_3)}} \right)^T. \quad (38)$$

4.2.2 1d-inhomogeneous field (Stern-Gerlach apparatus)

We shall consider now the case where the prepared particles pass through a Stern-Gerlach apparatus. Inside this apparatus, the field has a prevalent magnitude B_M along a constant direction λ and some small inhomogeneity inducing a magnetic force of magnitude $\mu_M B_F$ along the constant direction ν .

Outside the SG, the distribution (36) applies. The presence of a magnetic force in the SG activates the External Reset condition. We shall assume for

the sake of discussion that each node inside the SG hosts a magnetic-force boson and thus the first ER occurs right at the SG entry. There,

$$\mathbf{s} \leftarrow s \sum_{d=1}^3 |\mu_d| \lambda_d = s |\mathbf{s}|. \quad (39)$$

After the first ER, inside the SG, \mathbf{s} can only increase (resp., decrease) if $s = 1$ (resp., $s = -1$), as stated by (33). Consequently, since s_0 is source-defined and does not change with the iterations, s remains constant inside the SG. Solving (33) thus yields

$$\mathbf{s}[n] = \frac{A - e^{-2B_D s n}}{A + e^{-2B_D s n}}, \quad (40)$$

where $A = (1 + |s_\mu|)/(1 - |s_\mu|)$ and n is here the number of iterations counted from the SG entry. After a large number of iterations, \mathbf{s} converges toward s (and μ converges to $s\lambda$), see Fig. 4. Since the value of s is determined by the entry value s_μ , the probability of having a spin up at the exit of the apparatus is still given by (37).

The magnetic force along the ν direction is

$$f_\nu[n] = -\mu_M B_F \sum_{d=1}^3 \mu_d[n] \lambda_d = -\mu_M B_F \mathbf{s}[n]. \quad (41)$$

Integrating the rules of motion yields

$$\mathbf{v}_\nu[n] = \mu_M B_F n - \frac{s \mu_M B_F}{B_D} \log \left(\frac{A e^{2s B_D n} + 1}{A + 1} \right), \quad (42)$$

which, after a large number of iterations, tends to the continuous-time trajectory

$$-s \left(\mu_M B_F t + \frac{\mu_M B_F}{B_D} \log \left(\frac{1 + |s_\mu|}{2} \right) \right). \quad (43)$$

We retrieve in this way the standard SG behavior, with two symmetric beams separated along the $\pm\nu$ directions according to their value of s . Note, however, that w.r.t. the textbook trajectories $-s\mu_M B_F t$, a sort of time delay emerges, which can be quantified as

$$-\frac{1}{B_D} \log \left(\frac{1 + |s_\mu|}{2} \right), \quad (44)$$

see Fig. 4. Note that the time delay does not depend on the sign of s_μ .

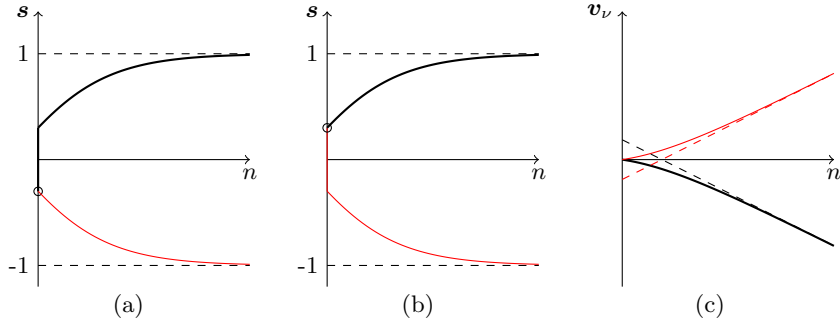


Fig. 4 Qualitative variation of s (a–b) and v_n (c) within an inhomogeneous magnetic field as a function of the number of iterations, for $s = 1$ (black) and $s = -1$ (red), $s_\mu < 0$ (a, c) and $s_\mu > 0$ (b, c). The circle represents the condition outside the apparatus. The vertical jump represents the first ER at the SG entry. The dashed lines represent the asymptotic behavior of momentum, leading to the textbook separation.

4.2.3 Numerical results

We shall consider a magnetic field arbitrarily oriented along the x_3 axis, with a one-dimensional inhomogeneity along the same direction, $B = (0, 0, B_1 x_3)$. Even if this field does not satisfy Maxwell equation $\nabla \cdot B = 0$, we choose it to simplify the notation. In fact, the literature has shown its equivalence to any “physical” field where the inhomogeneity is along one constant direction, provided that the two directions are exchanged [31]. The field is concentrated in a certain region of space along the propagation direction x_2 .

Ensemble results are compared with those of quantum mechanics (theoretical values) obtained by using the two-component propagator [31,32]

$$K^{(SG)}(x, t|x_0) = \frac{1}{(2\iota t)^{3/2}} \cdot \exp\left(\frac{\iota\pi(x-x_0)^2}{2t} + \frac{\iota\pi(x_1+x_{10})\sigma_3\phi t}{2} - \frac{\iota\pi\phi^2 t^3}{24}\right) \quad (45)$$

in lattice units, where σ_3 denotes here the Pauli matrix.

A Gaussian-wave preparation is considered, where sources are set to represent the bi-dimensional QM initial state

$$\psi_0(x_0) = \left(\frac{1}{\pi d_1 d_3}\right)^{1/2} \exp\left(-\frac{x_{01}^2}{2d_1^2} - \frac{x_{03}^2}{2d_3^2}\right). \quad (46)$$

By virtue of the equivalence (38), the initial polarizations are chosen as to represent an initial spin state $\chi_0 = (\chi_1, \chi_2)$,

$$\mu_{03} = \chi_1 \chi_1^* - \chi_2 \chi_2^*, \quad \mu_{01} = \chi_1 \chi_2^* + \chi_1^* \chi_2, \quad \mu_{02} = -\iota(\chi_1 \chi_2^* - \chi_1^* \chi_2), \quad (47)$$

where the asterisk denotes here complex conjugation.

The theoretically expected pdf is obtained numerically from the propagated spinor $\chi(x, t)$ as $\rho(x; t) = \chi^T \begin{pmatrix} 1 & 0 \\ 0 & 1 \end{pmatrix} \chi$. This pdf is to be compared

with the frequency of particle arrivals at nodes x after t iterations computed by the proposed model.

The theoretically expected spin density along the x_3 direction is obtained as $\langle S_3 \rangle(x; t) = \chi^T \begin{pmatrix} 1 & 0 \\ 0 & -1 \end{pmatrix} \chi$. This quantity is to be compared with its counterpart in the proposed model, obtained as the difference between the frequency of arrivals of particles with $s = 1$ ($\mu_3 = \lambda_3 = 1$) and of those with $s = -1$ ($\mu_3 = -\lambda_3 = -1$).

Figures (5)–(6) show the calculated spin density after $t = 64$ iterations for a source scenario with $\mu_M B_F = 0.1/\pi^2$, $d_1 = d_2 = 1$, $\chi_1 = \chi_2 = 1/\sqrt{2}$ (that is, $\mu_{01} = 1$ in the proposed model). Globally, these result match the theoretical values, which clearly show the textbook spin separation occurring along the inhomogeneity direction.

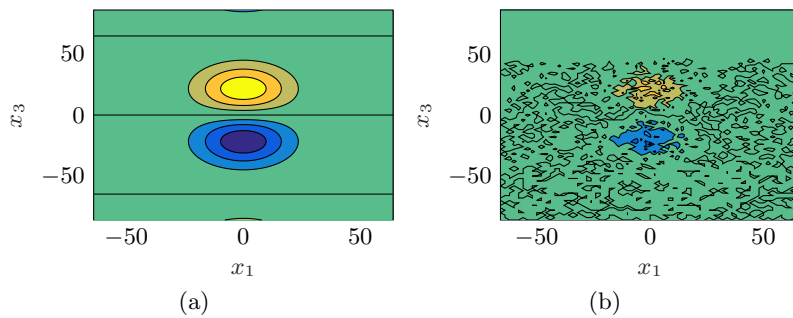


Fig. 5 Differential frequency of arrival (b) and theoretical spin density $\langle S_3 \rangle$ (a) for $N_p = 10000$, $t = 64$ as a function of position (Stern-Gerlach, Gaussian wave, $\mu_M B_F = 0.1/\pi^2$, $d_1 = d_3 = 1$, $\chi_1 = \chi_2 = 1/\sqrt{2}$).

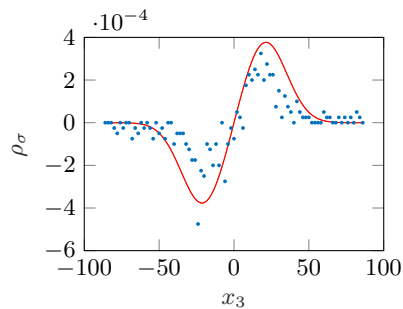


Fig. 6 Differential frequency of arrival (blue) and theoretical spin density (red) for $N_p = 10000$, $t = 64$ as a function of the inhomogeneity direction (Stern-Gerlach, Gaussian wave, $\mu_M B_F = 0.1/\pi^2$, $d_1 = d_3 = 1$, $\chi_1 = \chi_2 = 1/\sqrt{2}$).

5 Spin Entanglement

In [1] momentum entanglement has been described within the context of the Local-Realistic Model. Here we extend those results to the case of spin entanglement.

5.1 Particle emission

Entangled particles are emitted at sources as pairs ($n_R = 2$) and denoted with a superscript $R \in \{I, II\}$. In addition to assigning entangled momenta, the source preparation attributes entangled source spins, according to the rule $s_0^{(II)} + s_0^{(I)} = 0$. We shall denote, without loss of generality, $s_0^{(I)} = s_0$ and, consequently, $s_0^{(II)} = -s_0$, where $s_0 = U[-1, 1]$ as before. The same polarization $\mu_0^{(I)} = \mu_0^{(II)} = \mu_0$ is also randomly attributed to each particle at the source.

5.2 Microscopic motion

All rules described above remain the same in the case of entangled particles, except for the spin dynamics (30)–(31), which is generalized as

$$s^{(R)}[n] = \text{sign} \left(s_0^{(R)} + \mathbf{s}^{(R)}[n] \right) \quad (48)$$

$$\mathbf{s}^{(R)}[n] = \text{sign} \left(\sum_{d=1}^3 \mu_d^{(R)}[n] \lambda_d^{(R)}[n] \right) \cdot \left| \sum_{d=1}^3 \mu_d^{(R)}[n] \lambda_d^{(R)}[n] \right|^{n_R}. \quad (49)$$

Clearly, for $n_R = 1$, equation (31) is retrieved. We define for later use $s_\mu^{(R)} := \sum_{d=1}^3 \mu_{d0} \lambda_d^{(R)}$.

5.3 Probability densities

We aim at reproducing a Bell test experiment. Thus each particle of the same emission is sent to a SG apparatus oriented along the direction $\nu^{(R)}$, and thence to either of two “detectors” placed at a distance $\pm \delta_\nu^{(R)}$ along that direction.

We shall evaluate the joint pmf $\rho(s^{(I)}, s^{(II)})$, representing the probability that two entangled particles of the same emission arrive at the positions $-s^{(I)}\delta_\nu^{(I)}$, resp., $-s^{(II)}\delta_\nu^{(II)}$. We note that, experimentally, only coincidences in arrival time at these detectors can be recorded, see [23]. Therefore, the joint pmf describes only those particle pairs for which $x_\nu^{(I)}[n] = -s^{(I)}\delta_\nu^{(I)}$ and $x_\nu^{(II)}[n] = -s^{(II)}\delta_\nu^{(II)}$ at a given iteration n , where x_ν is the number of nodes along the direction ν . As already discussed in [1] in another context, for large number of particle emissions and large t and δ 's, we can replace x_ν with \mathbf{x}_ν , its expected value.

The quantities $\mathbf{x}_\nu^{(R)}$ can be explicitly evaluated as $\mathbf{x}_\nu^{(R)}(t) = \int \mathbf{v}_\nu^{(R)}(t)dt$, with $\mathbf{v}_\nu^{(R)}$ evaluated similarly to (42). It is thus apparent that $\mathbf{x}_\nu^{(R)} = \text{fcn}(t, s_0, |s_\mu^{(R)}|)$. While the other parameters of influence are common to both particles, it is the cosine term $s_\mu^{(R)} = \cos(\mu_0, \lambda^{(R)})$ that ultimately controls the momentum and thus the position reached along the respective SG directions. If we set, without loss of generality, $\delta_\nu^{(I)} = \delta_\nu^{(II)}$, then a coincidence in arrival times is expectedly recorded when the two particles have the same value of s_μ , that is,

$$s_\mu^{(I)} = \sum_{d=1}^3 \lambda_d^{(I)} \mu_{0d} = \sum_{d=1}^3 \lambda_d^{(II)} \mu_{0d} = s_\mu^{(II)} := s_\mu \quad (50)$$

It is now easy to show that, for each selection of $\lambda^{(I)}, \lambda^{(II)}$, two values of s_μ fulfill (50), namely,

$$\hat{s}_\mu = \pm \sqrt{\frac{1 + \sum_{d=1}^3 \lambda_d^{(I)} \lambda_d^{(II)}}{2}}, \quad (51)$$

having opposite signs and equal probability³. These values correspond to the particular choice $\hat{\mu}_0 = \pm(\lambda^{(I)} + \lambda^{(II)})/2$. All other values of μ_0 do not give rise to recorded coincidences (at least when considering only expected motion) and thus do not contribute to the joint pmf.

Similarly to the non-entangled case, inside the SG $s^{(R)}$ remains constant at the entry value $s^{(R)} = \text{sign}(s_0^{(R)} + \text{sign}(s_\mu)s_\mu^2)$. The distributions of $s^{(R)}$ are therefore found as

$$s^{(I)} = \begin{cases} 1, & s_0 > -\text{sign}(s_\mu)s_\mu^2 \\ -1, & s_0 < -\text{sign}(s_\mu)s_\mu^2 \end{cases} \quad (52)$$

and

$$s^{(II)} = \begin{cases} 1, & s_0 < \text{sign}(s_\mu)s_\mu^2 \\ -1, & s_0 > \text{sign}(s_\mu)s_\mu^2 \end{cases} \quad (53)$$

With the help of Fig. 7, we further note that $\{s^{(I)}, s^{(II)}\} = \{1, 1\}$ for $s_0 \in [-s_\mu^2, s_\mu^2]$ if $s_\mu > 0$. Likewise, $\{s^{(I)}, s^{(II)}\} = \{-1, -1\}$ for $s_0 \in [-s_\mu^2, s_\mu^2]$ if $s_\mu < 0$. Conversely, $\{s^{(I)}, s^{(II)}\} = \{-1, 1\}$ for $s_0 < -s_\mu^2$ and $\{s^{(I)}, s^{(II)}\} = \{1, -1\}$ for $s_0 > s_\mu^2$.

Finally, remembering that $\rho(s_0) = 1/2$, the joint distribution is evaluated as

$$\rho(1, 1) = \Pr(s_\mu > 0) \cdot \frac{2s_\mu^2}{2} = \frac{s_\mu^2}{2} \quad (54)$$

$$\rho(-1, -1) = \Pr(s_\mu < 0) \cdot \frac{s_\mu^2}{2} = \frac{s_\mu^2}{2} \quad (55)$$

$$\rho(1, -1) = \frac{1 - s_\mu^2}{2} = \rho(-1, 1). \quad (56)$$

³ Geometrically, they correspond to the two unit μ_0 vectors bisecting the angle between the two directions $\lambda^{(I)}, \lambda^{(II)}$.

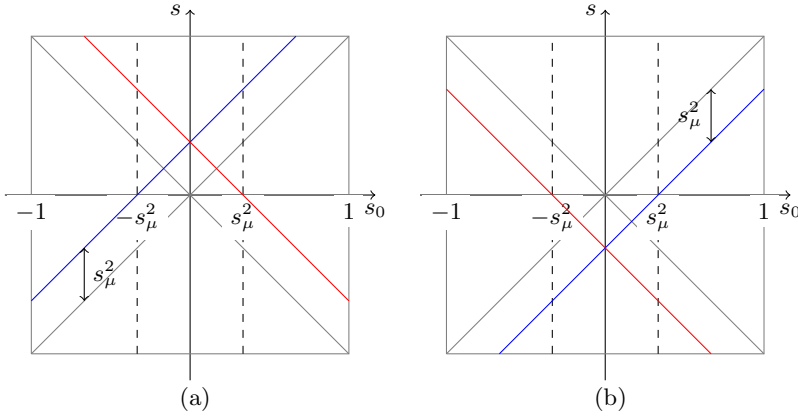


Fig. 7 Illustration of the quantities $s_0^{(I)} + \text{sign}(s_\mu)s_\mu^2$ whose sign is $s^{(I)}$ (blue) and $s_0^{(II)} + \text{sign}(s_\mu)s_\mu^2$ whose sign is $s^{(II)}$ (red) after the ER as a function of s_0 , for $s_\mu > 0$ (a) and $s_\mu < 0$ (b).

Since from (51) the only meaningful value is $\hat{s}_\mu^2 = (1 + \cos(\lambda^{(I)}, \lambda^{(II)}))/2$, the joint distribution reads

$$\rho(s^{(I)}, s^{(II)}) = \frac{1 + s^{(I)}s^{(II)} \cos(\lambda^{(I)}, \lambda^{(II)})}{4}, \quad (57)$$

that is, precisely the QM prediction.

Note that, although μ_0 plays the role of a hidden variable as those explicitly discarded by Bell's theorem, the pdf (57) is not in the form postulated by this theorem. In fact, (57) is generally not factorized as the product of two (bivalued) terms, separately depending on $\lambda^{(I)}$ and $\lambda^{(II)}$ (a Bell's assumption often referred to as setting independence or no-signaling [33]) albeit possibly from a common set of hidden variables. Therefore, the proposed model is not forbidden by Bell's theorem, which is based on Bell's assumptions, to violate Bell's inequalities.

Nevertheless, nowhere in the proposed model, particles, say, II know about which magnetic field experience particles I, thus locality still applies even if the setting independence assumption is not valid. The emergence of a particular polarization μ_0 that is a function of both $\lambda^{(I)}$ and $\lambda^{(II)}$ results from the fact that for other values of μ_0 , the desired combination of $x_\nu^{(I)}$ and $x_\nu^{(II)}$ at the same iteration is impossible or, at least, highly improbable. In this respect, the key feature of the proposed model is the dependency of the particle trajectories on two random hidden variables (s_0 and μ_0).

5.4 Numerical Results

We aim at representing here a textbook two-channel Bell test experiment. A source produces pairs of entangled particles, sent in opposite directions. Each

particle beam encounters a SG. Emerging particles from each channel are detected and coincidences in arrivals counted. Similarly to the non-entangled scenario simulated in Sect. 4.2.3, we shall take $\lambda^{(R)} = \nu^{(R)}$, i.e., without loss of generality, an inhomogeneity directed along the field in both SG. While the orientation $\lambda^{(I)}$ is fixed, $\lambda^{(I)}$ is varied between $-\pi$ and π in the plane x_1 - x_2 . The direction of the two emitted beams is taken as $\pm x_3$. Ensemble results are compared with QM prediction (57).

In the proposed model, particles are emitted at the source according to a Gaussian-wave preparation, with $m_1 = m_2 = 0$, while m_3 determines the average particle speed along the two beams. We assume that the time spent before encountering the respective SG is sufficient to complete both the “lattice training” and the “particle training” processes discussed in [1]. In other terms, before the SG entry, the momentum propensities in the 1,2 directions have already converged to their stationary distributions. Therefore, and by virtue of the discussion in Sect. 2.4.1, we have directly set $\mathbf{v}_1 = \mathbf{v}_2 = 0$. The polarization vector is randomly chosen at each emission between N_μ possible values, equally spaced between $\angle \hat{\mu}_0$ and $\angle \hat{\mu}_0 + 2\pi$. The particles are assumed to spend a time t_{SG} (defined by m_3) in their respective SGs. After this time, they emerge in regions without external forces, so that the momentum propensities acquired inside the SG are conserved. Coincidences are registered when particles arrive at either of a pair of detectors after t iterations. The detector locations vary as a function of the field angular difference and are chosen as to capture the largest number of particles, i.e., they are set to $\pm (\mathbf{x}_\nu(t_{SG}|1, \hat{s}_\mu) + \mathbf{v}_\nu(t_{SG}|1, \hat{s}_\mu) \cdot (t - t_{SG}))$, with a tolerance of ± 2 nodes. Frequency of coincidences of each type are calculated as the number of coincidences of that type divided by the total number of coincidences.

Figure 8 shows the frequency of the four types of coincidences as a function of the angular difference between the two fields after $t = 150$ iterations, with $\mu_M B_F = 0.01$, $B_D = 0.05$, $N_p = 1 \cdot 10^5$, $N_\mu = 16$, $t_{SG} = 50$. When compared with the QM predictions, these results confirm the substantial equivalence of the two models as anticipated in the previous section.

6 Conclusions

The paper has shown how nonrelativistic QM including spin can be reproduced with realistic, stochastic, and localistic motion rules of individual particles. QM predictions are indeed retrieved as probability distributions of position, momentum, angular momentum, spin, etc. without appealing to the QM mathematical machinery itself.

Concerning angular momentum, typical QM phenomena, and quantization in particular, are naturally described within the set of rules already described in [1] and further detailed in this paper.

To represent spin scenarios, such as Stern-Gerlach apparatuses or a Bell test experiment, the proposed model does not appeal to two-dimensional complex spinors and matrices but uses a relatively simple set of rules, implying that (1) spin is a dichotomic quantity carried on by particles whose value depends on a random source setting and a spin propensity; (2) the latter

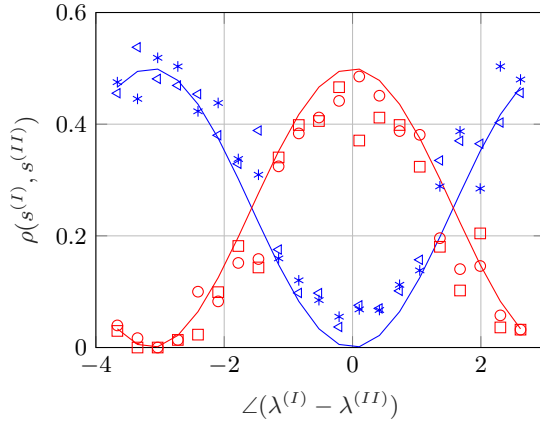


Fig. 8 Frequency of coincidences of arrivals (1,1) (circles), (-1,-1) (squares), (1,-1) (stars), and (-1,1) (triangles), with their theoretical values $\rho(1,1) = \rho(-1,-1)$ (red solid) and $\rho(1,-1) = \rho(-1,1)$ (blue solid) as a function of the angle (rad) between $\lambda^{(I)}$ and $\lambda^{(II)}$ (Bell experiment, Gaussian-wave beams,).

can vary at each iteration as a function of polarization, which is a three-dimensional attribute, and the magnetic field experienced; (3) polarization is randomly attributed during preparation and has its own rules of change; it further concurs in determining how particles react to magnetic fields.

Overall, observables are described by variables (integer- or rational-valued) that are attributed to the particles or to the lattice. These attributes are subject to stochastic preparation at sources and time evolution, leading to their description in probabilistic terms (pdf or pmf). QM states are represented by the statistical properties of source quantities (position, momentum, phase, spin, polarization). To describe states dynamics, Schrödinger equation is replaced by the microscopic rules of motion, including the action of both external and quantum forces. The distribution of external “bosons” embodies the information that in QM is carried by the Hamiltonian. Born rule to find the pdf or the pmf of a certain observable is replaced by integral formulas such as (22). Stationary states are retrieved as those states whose pdf does not vary with time. Depending on the scenario, quantization of momentum, energy, and angular momentum may arise when their respective pdfs tend to a staircase function with peak values. With coupled source spin and polarization, spin-entangled particles are incorporated in the model that, despite being local and realistic, is thus able to violate the Bell-CHSH inequalities.

Several refinements of the model are still possible. For example, relativistic Newtons second law shall inspire a mechanism to prevent that the momentum propensity becomes larger than unity under the action of persistent forces. Multi-state and manyparticle systems are yet to be fully studied, too.

References

1. Sciarretta A.: A local-realistic model of quantum mechanics based on a discrete spacetime. *Found. Phys.* 48(1), 60–91, (2018)
2. Sciarretta, A.: A local-realistic model of quantum mechanics based on a discrete spacetime (extended version) (2017). <https://doi.org/10.13140/RG.2.2.17755.05925>, arXiv:1712.03227
3. Santos, E.: Towards a realistic interpretation of quantum mechanics providing a model of the physical world. *Found. Sci.* 20(4), 357-386 (2015)
4. Harrigan, N., Spekkens, R.W.: Einstein, incompleteness, and the epistemic view of quantum states. *Found. Phys.* 40, 125-157 (2010)
5. Einstein, A., Podolsky, B., Rosen, N.: Can quantum-mechanical description of physical reality be considered complete? *Phys. Rev.* 47, 777-780 (1935)
6. DEspagnat, B.: Quantum physics and reality. *Found. Phys.* 41, 1703-1716 (2011)
7. Bohm, D., Hiley, B.J.: *The Undivided Universe: An Ontological Interpretation of Quantum Theory.* Routledge, London (1993)
8. Floyd, E.: Welcher weg? A trajectory representation of a quantum diffraction experiment. *Found. Phys.* 37(9), 1403-1420 (2007)
9. Feynman, R.P., Hibbs, A.R.: *Quantum Mechanics and Path Integrals.* McGraw-Hill, New York (1965)
10. 13. Ord, G.N.: The Schrödinger and diffusion propagators coexisting on a lattice. *J. Phys.A*29, L123-L128 (1996)
11. Ord, G.N., Deakin, A.S.: Random walks, continuum limits and Schrödinger's equation. *Phys. Rev. A* 54, 3772-3778 (1996)
12. Ord, G.N.: Schrödinger's equation and classical Brownian motion. *Fortschr. Phys.* 46(68), 889-896 (1998)
13. Janaswamy, R.: Transitional probabilities for the 4-state random walk on a lattice. *J. Phys. A* 41, 1-11 (2008)
14. Badiali, J.P.: Entropy, time-irreversibility and the Schrödinger equation in a primarily discrete spacetime. *J. Phys. A* 38(13), 2835-2848 (2005)
15. Nelson, E.: *Quantum Fluctuations.* Princeton University Press, Princeton (1985)
16. Nottale, L.: *Fractal Space-Time and Microphysics.* World Scientific, Singapore (1996)
17. Nagasawa, M.: *Schrödinger Equations and Diffusion Theory.* Birkhauser Verlag, Basel (1993)
18. Fritsche, L., Haugk, M.: A new look at the derivation of the Schrödinger equation from Newtonian mechanics. *Ann. Phys. (Leipzig)* 12(6), 371-403 (2003)
19. Carroll, R.: Remarks on the Schrödinger equation. *Int. J. Evol. Equ.* 1, 23-56 (2005)
20. Grössing, G.: Sub-quantum thermodynamics as a basis of emergent quantum mechanics. *Entropy* 12, 1975-2044 (2010)
21. Jin, F., Yuan, S., De Raedt, H., Michielsen, C., Miyashita, S.: Corpuscular model of two-beam interference and double-slit experiments with single photons. *J. Phys. Soc. Jpn.* 79(7), 074401114 (2010)
22. Michielsen, K., De Raedt, H.: Event-based simulation of quantum physics experiments. *Int. J. Mod. Phys. C* 25(8), 1430003 (2014)
23. De Raedt, K., de Raedt, H., Michielsen, K.: A computer program to simulate EinsteinPodolsky RosenBohm experiments with photons. *Comput. Phys. Commun.* 176(1112), 642-651 (2007).
24. Khrennikov, A., Volovich, Y.I.: Discrete time dynamical models and their quantum-like context dependent properties. *J. Modern Opt.* 51(6/7), 113-114 (2004)
25. Dowker, F., Henson, J.: Spontaneous Collapse Models on a Lattice. *J. Stat. Phys.* 115(516), 1327-1339 (2004)
26. Bialynicki-Birula, I.: Weyl, Dirac, and Maxwell equations on a lattice as unitary cellular automata. *Phys. Rev. D* 49(12), 6920-6927 (1994)
27. Couder, Y., Bouadoud, A., Protire, S., Fort, E.: Walking droplets: a form of waveparticle duality at macroscopic level? *Europhys. News* 41(1), 14-18 (2010)

-
28. Nielsen, H.B. and Rohrlich, D.: A path integral to quantize spin. *Nuclear Physics B* 299, 471–483 (1988)
 29. Dankel, T.: Mechanics on Manifolds and the Incorporation of Spin into Nelson's Stochastic Mechanics. *Arch. Rational Mech. Anal.* 37, 192–221 (1970)
 30. Garbaczewski, P.: Randomness in the Quantum Description of Neutral Spin $1/2$ Particles, *Fortschr. Phys.* 38(6), 447–475 (1990)
 31. Hsu, B., Berrondo, M., Van Huele, J.-F.: Stern-Gerlach dynamics with quantum propagators. *Phys. Rev. A* 83, 012109 (2011).
 32. Reddy, A., Samuel, J., Shivam, K., Sinha, S.: Coarse Quantum Measurement: An analysis of the SternGerlach experiment, *Phys. Lett. A* 380, 1135-1140 (2016)
 33. Di Lorenzo, A.: Beyond Bells theorem: admissible hidden-variable models for the spin-singlet. *J. Phys.* 442, 012046 (2013).